

SalientDSO: Bringing Attention to Direct Sparse Odometry

Huai-Jen Liang, Nitin J. Sanket, Cornelia Fermüller, Yiannis Aloimonos

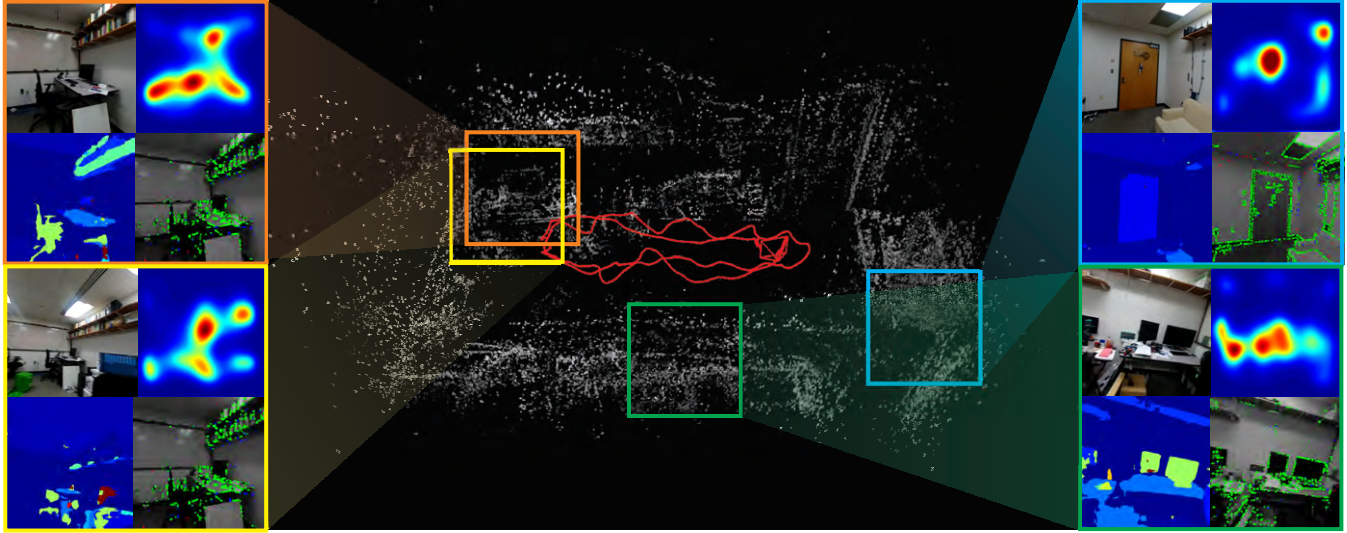


Fig. 1: Sample point-cloud output of SalientDSO which does not have loop closure or global bundle adjustment. The insets show the corresponding image, saliency, scene parsing outputs and active features. Observe that features from non-informative regions are almost removed approaching object centric odometry.

Abstract—Although cluttered indoor scenes have a lot of useful high-level semantic information which can be used for mapping and localization, most Visual Odometry (VO) algorithms rely on the usage of geometric features such as points, lines and planes. Lately, driven by this idea, the joint optimization of semantic labels and obtaining odometry has gained popularity in the robotics community. The joint optimization is good for accurate results but is generally very slow. At the same time, in the vision community, direct and sparse approaches for VO have stricken the right balance between speed and accuracy.

We merge the successes of these two communities and present a way to incorporate semantic information in the form of visual saliency to Direct Sparse Odometry – a highly successful direct sparse VO algorithm. We also present a framework to filter the visual saliency based on scene parsing. Our framework, *SalientDSO*, relies on the widely successful deep learning based approaches for visual saliency and scene parsing which drives the feature selection for obtaining highly-accurate and robust VO even in the presence of as few as 40 point features per frame. We provide extensive quantitative evaluation of SalientDSO on the ICL-NUIM and TUM monoVO datasets and show that we outperform DSO and ORB-SLAM – two very popular state-of-the-art approaches in the literature. We also collect and publicly release a CVL-UMD dataset which contains two indoor cluttered sequences on which we show qualitative evaluations. To our knowledge this is the first paper to use visual saliency and scene parsing to drive the feature selection in direct VO.

All authors are associated with University of Maryland, College Park. Emails: {hjliang@terpmail, nitin@umiacs, fer@umiacs, yiannis@umiacs}@.umd.edu

Keywords – Visual Saliency, Scene Parsing, Direct Sparse Odometry, SLAM.

SUPPLEMENTARY MATERIAL

The accompanying video and dataset is available at prg.cs.umd.edu/SalientDSO.html.

I. INTRODUCTION AND PHILOSOPHY

Simultaneous Localization and Mapping (SLAM) and Visual Odometry (VO) algorithms have taken center stage in the recent years due to their wide-spread usage. They play a prominent part in the perception and planning pipelines of self-driving cars, autonomous quadrotors, augmented and virtual reality. The never ending quest to come up with realtime solutions for these methods whilst being as accurate as their offline counterparts has led to alternative problem formulations in terms of constraints and optimization methods [1]–[4].

Not so long ago, the field was dominated by indirect methods [1], [2], [5], [6] which rely on feature matching and foundations of multi-view geometry coupled with windowed optimization to build a map of the scene and obtain accurate poses. These approaches are based on the low-level geometric features and do not work very well with environments with repeating structures and texture-less surfaces. Some works have improved upon the previous approaches in-terms of speed and accuracy by incorporating

prior knowledge such as the dynamics of the system and/or data from more sensors such as inertial measurement units [7], time-of-flight sensors [8] etc. However, minimalism is a trend forward, i.e., trying to achieve the same tasks with a minimal number of sensors. In the scope of this paper, we focus on a monocular VO solution. The current state-of-the-art in monocular approaches which have the best compromise of speed and accuracy are direct sparse approaches such as Direct Sparse Odometry (DSO) [9].

However, object centric SLAM approaches are more robust by nature due to the high level semantics used in the formulation. Lately, joint optimization of 3D poses, structure and labelled object locations has improved the state-of-the-art significantly. These frameworks rely on the widely successful deep learning based object recognition engine and pose graph optimization frameworks, combining both low-level geometric features and the high-level semantics.

However, humans perform the task of mapping very differently. The human visual system interprets the scene for various tasks like recognition, segmentation, tracking and navigation by making a series of fixations [10]. This is called the Active approach [11]–[13], whilst the traditional approach is called the Passive approach (See Table I). These fixations lie in the proto-segmentation of the salient objects/locations in the scene. The word proto-segmentation refers to the fact that a segmentation around the fixation point may lead to partial/complete segmentation of an object, which depends on the scenario. Solving the problem of recognition and tracking along with segmentation is like a chicken-egg problem. One would need a good segmentation for recognition and tracking and vice-versa. An Expectation-Maximization (EM) type of scheme, where one would jointly/alternatively optimize for the segmentation and recognition/tracking has gained popularity in literature lately, due to the advancement of fast and accurate optimization frameworks.

Very recently, this philosophy of fixation and attention has started to gain popularity in the robot navigation community [14]–[17]. This is based on the fact that humans perform the task of mapping very differently from how it has been done in the robotics literature. They build “semantic/topological” maps to traverse the scene. This paper combines the concepts used by humans and robotics literature to present a framework of indoor visual odometry in which the features are selected based on a visual saliency map that is obtained by human eye tracking data. This work aims to mimic the qualitative human vision in the framework of direct VO. The key contributions of this paper are:

- We present a framework of indoor visual odometry in which the features are selected based on a visual saliency map (Sample output is shown in Fig. 1).
- We present a method to filter saliency map based on scene parsing.
- We provide experimental results on various simulated and real indoor environments to demonstrate the improved performance of the proposed approach with

TABLE I: Active vs Passive approach for computer vision tasks.

Task	Passive approach	Active approach
Segmentation	Graph cut or super-pixel based methods.	Fixation based region segmentation and recognition in a feedback loop.
Recognition	Sliding window of filter banks with a classification algorithm for final prediction.	Saliency/fixation based segmentation/clustering followed by selection of attributes and sliding window of filters with a simple classification algorithm.
Tracking and Failure recovery	Making an online dictionary for robustness against changes and use detection for failure recovery.	Tightly couple saliency into the tracking filter to reduce search space and use salient regions for failure recovery. By doing so, we introduce high level semantics into the low level processes (feedback).
Navigation and Mapping	Map based on features based on image gradients.	Map only using salient region features or objects obtained using fixation based segmentation. Take advantage of the semantic relationships between differently labeled regions.

comparisons to the state-of-the-art.

The rest of the paper is organized as follows: Sec. II presents the different parts of the proposed SalientDSO framework along with the preliminaries required. Sec. III describes the visual saliency and scene parsing driven point selection algorithm used in SalientDSO. Detailed experiments along with quantitative and qualitative results are given in Sec. IV. We finally conclude the paper in Sec. V with parting thoughts on future work.

II. SALIENTDSO FRAMEWORK

SalientDSO’s framework is composed of a pre-processing step and a VO backbone. The VO backbone is responsible for initializing and tracking camera pose and optimizing all model parameters. The pre-processing step involves the saliency prediction and scene parsing using deep Convolutional Neural Networks (CNNs) and later using these outputs to select features/points. Fig. 2 shows the algorithmic overview of SalientDSO, where blue parts of the figure show our contributions (which constitute the pre-processing step). Each component of SalientDSO is discussed in detail next.

A. Visual Odometry Backbone

We adopt DSO [9] as the backbone VO in SalientDSO. In brief, DSO [9] proposed a direct sparse model to jointly optimize all parameters (camera intrinsics, camera extrinsics, and inverse-depth values for feature points) and perform windowed bundle adjustment. It contains a front end for frames/points selection and initialization, and a back end for optimization. In the proposed framework, points selection is replaced with our proposed method in Sec. III-C. The front-end and back-end are detailed next.

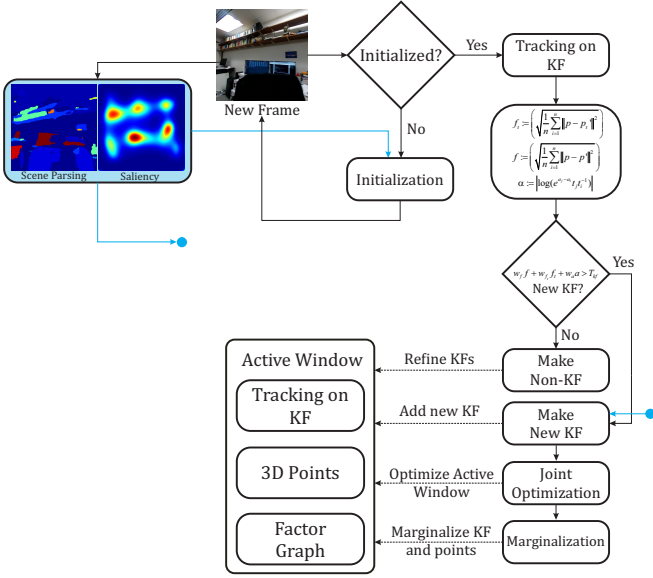


Fig. 2: Algorithmic overview of SalientDSO, blue parts show our contributions.

1) *Front-end*: The front-end part of algorithm handles the following:

Initial Frame Tracking: A new frame is tracked with respect to the latest KeyFrame (KF) by using the conventional two-frame direct image alignment, a multi-scale image pyramid and a constant motion model. If tracking fails, SalientDSO attempts to recover the motion by trying 27 different small rotations.

Keyframe Creation: Similar to ORB-SLAM [5], SalientDSO initially takes many keyframes (around 5-10 keyframes per second), and then sparsifies them by early marginalization of the redundant KFs. SalientDSO uses the following three rules to decide if a new KF is needed: mean square optical flow $\left(f_t := \left(\frac{1}{n} \sum_{i=1}^n \|p - p_t'\|^2\right)^{0.5}\right)$, mean flow without rotation $\left(f := \left(\frac{1}{n} \sum_{i=1}^n \|p - p'\|^2\right)^{0.5}\right)$ and relative brightness factor $\left(\alpha := \left|\log \left(e^{a_j - a_i} t_j t_i^{-1}\right)\right|\right)$. A new KF is chosen when $w_f f + w_t f_t + w_a a > T_{kf}$. Here the symbols have the same meaning as in [9].

Candidate point tracking: Candidate points are selected using the approach described in Sec.III-C. These points are then tracked using discrete search along epipolar line and minimizing the photometric error E_{photo} given by Eq. 3. The computed depth and co-variance is used to constrain the search interval for the subsequent frame as described in [18].

Outlier rejection and occlusion detection: Point observations which have a E_{photo} above a certain threshold are removed as outliers and excluded for further computation.

Parameters initialization: This step provides the initial estimates of all parameters for optimizing the non convex error E_{photo} . The initial camera pose is computed from direct image alignment and the initial point's depth is from candidate point tracking.

Candidate point activation: New candidates points

replace the old marginalized points. The new points are chosen by projecting onto the current frame and maximizing the distance between projection of any existing active points.

Marginalization: This step decides which points and frames should be marginalized. A KF will be marginalized if less than 5% of points are visible in the latest frame. If there are more than N_f (fixed at 7) KFs, a KF which is far from current frame and close to any other KFs will be marginalized.

2) *Back-end*: The back end contains a factor graph which performs continuous windowed optimization using the approach given in [19]. It optimizes E_{photo} using Gaussian-Newton algorithm in a sliding window manner. The error functions are defined as the following:

For a single active point p , its photometric error on KF j is defined as:

$$E_{pj} = \sum_{p \in N_p} w_p \left\| \left(I_j[p'] - b_j \right) - \frac{t_j e^{a_j}}{t_i e^{a_i}} \left(I_i[p] - b_i \right) \right\|_{\gamma} \quad (1)$$

where p' is the projection of point p on KF j , $\{t_i, t_j\}$ are the exposure time for images $\{I_i, I_j\}$, $\|\cdot\|_{\gamma}$ is the Huber norm, a_i, a_j, b_i, b_j are brightness transfer function parameters, N_p is the residual pattern with eight surrounding neighbors and gradient depending weights w_p is given by

$$w_p = \frac{c^2}{c^2 + \|\nabla I_i(p)\|_2^2} \quad (2)$$

The full photometric error over all active points and KFs is defined as

$$E_{photo} = \sum_{i \in F} \sum_{p \in P_i} \sum_{j \in obs(p)} E_{pj} \quad (3)$$

where F indicates all active KFs, P_i indicates all active points in KF i , $obs(p)$ indicates all frames' observation in which point p is visible.

III. POINT SELECTION BASED ON VISUAL SALIENCY AND SCENE PARSING

A. Visual Saliency Prediction

Visual saliency is defined as the amount of attention a human would give to each pixel in an image. This is quantitatively measured as the average time a person's gaze rests on each pixel in the image. Prediction of saliency is a hard problem and data driven approaches have lately excelled at this task. We adopt SalGAN [20] for saliency prediction in SalientDSO. In brief, SalGAN introduced the use of Generative Adversarial Network (GAN) [21] for saliency prediction. It contains a generator and a discriminator. The generator is a deep CNN trained on adversarial loss (L_{GAN} in Eq. 4), which includes Binary Cross-Entropy loss (L_{BCE} in Eq. 5) to produce a down-sampled saliency map, and the discriminator is a shallower network as compared to the generator, this is trained to solve binary classification between saliency map produced by generator and the

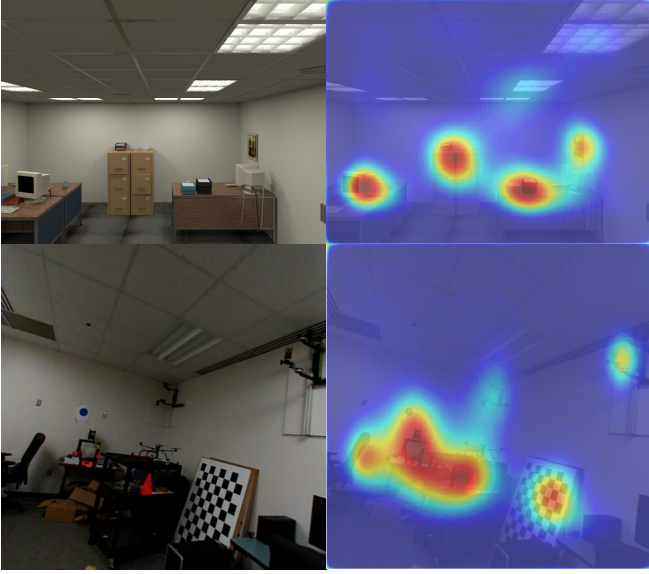


Fig. 3: Left column: Input image, Right column: Saliency overlaid on input image.

groundtruth. The generator is an encoder-decoder type of network, in which the encoder part is identical to VGG-16 [22] and its weights are initialized with the weights trained on the ImageNet dataset [23]. The discriminator’s weights are randomly initialized. The whole network is trained on the SALICON dataset [24].

The adversarial loss is defined as:

$$L_{GAN} = \alpha \cdot L_{BCE} - \log D(I, \hat{S}) \quad (4)$$

where $D(I, \hat{S})$ is the probability of fooling the discriminator. Also, the binary cross-entropy loss between the predicted saliency map \hat{S} and the ground-truth S is defined as:

$$L_{BCE} = -\frac{1}{N} \sum_{j=1}^N S_j \log(\hat{S}_j) + (1 - S_j) \log(1 - \hat{S}_j) \quad (5)$$

where S_j is the probability of pixel I_j being fixated.

Some sample results are shown in Fig. 3. One can clearly notice that walls, floors, and ceilings have lower probability of being fixated on, which is the main idea of the proposed framework.

B. Filtering saliency using semantic information

The saliency produced by SalGAN is concentrated around a fixation point inside the object and is fuzzy. Moreover, the saliency map is not very robust to viewpoint and illumination changes as the fixation point does not remain constant. In this subsection, we utilize semantic information to filter the saliency. The idea is to weigh down the saliency of uninformative regions, such as walls, ceilings and floors.

To obtain semantic information from a scene, we adopt Pyramid Scene Parsing [25] for retrieving semantic labels of every pixel in an image. In brief, Pyramid Scene Parsing (PSPNet) is a deep neural network for pixel-level prediction tasks. PSPNet uses CNN layers to extract features, then

Algorithm 1: Saliency prediction and filtering.

Data: Input image I , Pre-defined weights w_C

Result: Predicted final saliency \hat{S}^{final}

```

1  $\hat{S} = \text{SalGAN}(I)$ ;
2  $C = \text{PSPNet}(I)$ ;
3 for  $\forall \{x_j, y_j\} \in I$  do
4    $\hat{S}_j^{\text{weighted}} = w_C(C_j) \hat{S}_j$ ;
5 end
6 for  $\forall \{x_j, y_j\} \in I$  do
7    $\hat{S}_j^{\text{final}} = \text{median} \{ \hat{S}_i^{\text{weighted}}, \forall i \in C_j \}$ ;
8 end

```

a pyramid parsing module is applied to harvest different sub-region representation, followed by up-sampling and concatenation layers to form the final feature representation. The final features are then fed into more CNN layers to obtain a pixel-level prediction.

Once the per-pixel semantic information C is obtained, the predicted saliency map \hat{S} is filtered by:

$$\hat{S}_j^{\text{weighted}} = w_C(C_j) \hat{S}_j \quad (6)$$

Here, w_C are the predefined weights obtained empirically for different classes. To smooth and maintain a consistent saliency map for each class, each pixel is replaced by the median of saliency for its respective class:

$$\hat{S}_j^{\text{final}} = \text{median} \{ \hat{S}_i^{\text{weighted}}, \forall i \in C_j \} \quad (7)$$

All steps to generate \hat{S}^{final} are summarized in Algorithm 1.

C. Features/Points selection

Instead of uniformly selecting candidate points from an image as in DSO, we select points based on saliency. This is very helpful where the scene has a lot of objects or clutter which can be found generally in indoor scenes.

First, we split an image into $K \times K$ patches. For a patch M_i , we not only compute the median of gradient as a region-adaptive threshold, but also compute the median of saliency as a region-adaptive sampling weight sw_i . Therefore, for each patch, the sampling weight sw_i is computed as:

$$sw_i = \text{median} \{ \hat{S}_j^{\text{final}}, \forall j \in M_i \} + s_{\text{smooth}} \quad (8)$$

where s_{smooth} is a laplacian smoothing term used to control the bias on a salient region and the probability of a patch M_i being sampled is:

$$P_S(M_i) = \frac{sw_i}{\sum_{m \in M} sw_m} \quad (9)$$

Secondly, once a patch M_i has been selected, we further split M_i into $d \times d$ blocks. For each block, we select the pixel with the highest gradient only if it surpasses the region-adaptive threshold. With this strategy, we can select points which are well distributed in this salient region. In order to extract information from where no high-gradient

Algorithm 2: Saliency based points selection.

Data: Desired number of points N_{des} , s_{smooth} , \hat{S}^{final} **Result:** Selected points

```
1 Initialize selected point set as  $\{\emptyset\}$ ,  $N_{sel} = 0$ ;  
2 while  $N_{sel} < N_{des}$  do  
3   Randomly select a patch  $M$  from distribution  $P_S$ ;  
4   Split  $M$  into  $d \times d$  blocks;  
5   for each  $4d \times 4d$  block do  
6     for each  $2d \times 2d$  block do  
7       for each  $d \times d$  block do  
8         Select a point with the highest gradient  
          which surpass the gradient threshold;  
9       end  
10      if no selected point in this block then  
11        Select a point with the highest gradient  
          which surpass the weaker gradient  
          threshold;  
12      end  
13    end  
14    if no selected point in this block then  
15      Select a point with the highest gradient  
          which surpass the much weaker gradient  
          threshold;  
16    end  
17  end  
18   $N_{sel} = N_{sel} +$  the number of selected points;  
19 end
```

pixels are present, we follow the same approach as DSO and run two more passes to select pixels with weaker gradient in a larger sub-region with a lower gradient threshold and an increased d . A summary of the whole selection method is given in Algorithm 2.

Fig. 4 shows the selected points for some example scenes. We compare our selection based on saliency to the uniform selection adopted by DSO. One can easily notice that texture-less and mostly identical parts, such as walls, floors and ceilings, are down weighted in our pipeline. As demonstrated in Section IV, this helps us trade the weak features on the floors and ceilings for weak features on objects where the saliency is generally higher - thus, in-turn, making the feature selection more robust and object-centric.

IV. EXPERIMENTAL RESULTS AND ANALYSIS

In this section, we comprehensively evaluate SalientDSO on various datasets.

- **ICL-NUIM dataset** [26]: This dataset provides two scenes and four different trajectories for each scene which are obtained by running Kintinuous on real image data and finally used in a synthetic framework for obtaining ground-truth.
- **TUM monoVO dataset** [27]: This dataset provides 50 sequences comprising over 100 minutes videos. It ranges from indoor corridors to wide outdoor scenes. In our experiments, we only evaluate all methods on indoor

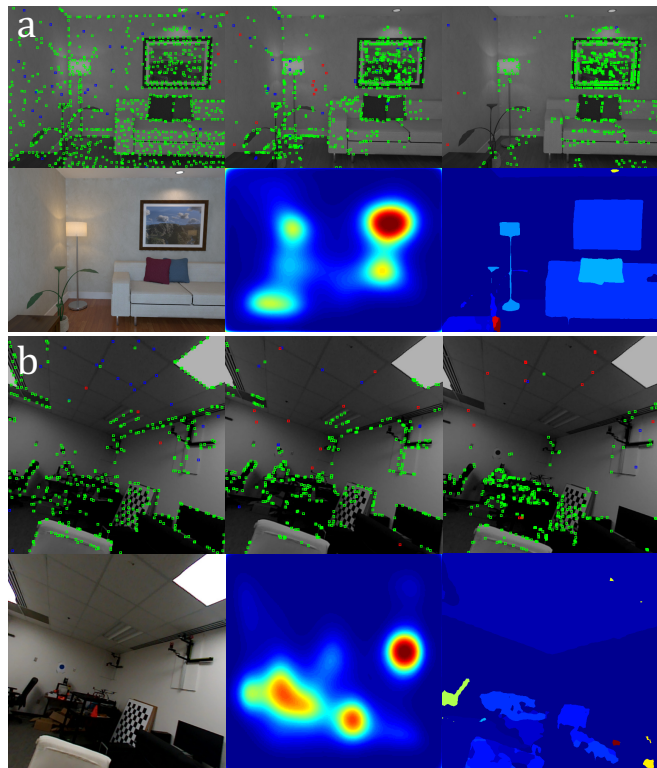


Fig. 4: Point selection using different schemes. Top rows in (a) and (b), left to right: features selected using DSO’s scheme, saliency only, saliency+scene parsing. Bottom rows in (a) and (b), left to right: input image, saliency, scene parsing output. Notice how using saliency+scene parsing removed all non-informative features.

TABLE II: Parameter settings for different datasets.

	TUM	ICL-NUIM	CVL
Num of active keyframes N_f	7	7	7
Num of active points N_p	2000	2000	1200
Global gradient constant g_{th}	7	3	7
Patch size K	8	8	8
Photometric correction	Yes	Not required	Not available

sequences $\{\text{sequence}_{(1-18, 26, 28, 35-38, 40)}\}$. Only the indoor sequences are chosen because the usage of saliency obtained by human gaze is meaningful only for indoor cluttered scenes.

- **CVL dataset:** This dataset was collected by the authors of this paper is available at prg.cs.umd.edu/SalientDSO.html. The data was collected using a Parrot® SLAMDunk [28] sensor suite. The data from the left camera is used in the experiments.

Different parameters used for running the experiments are shown in Table. II. For ICL-NUIM dataset, photometric correction is not required. To comprehensively evaluate the proposed method, we run each sequence in both forward and backward direction 10 times.

A. Quantitative Evaluation

Fig. 5 shows the absolute trajectory Root Mean Square Error (RMSE_{ate}) on ICL-NUIM dataset. Using visual

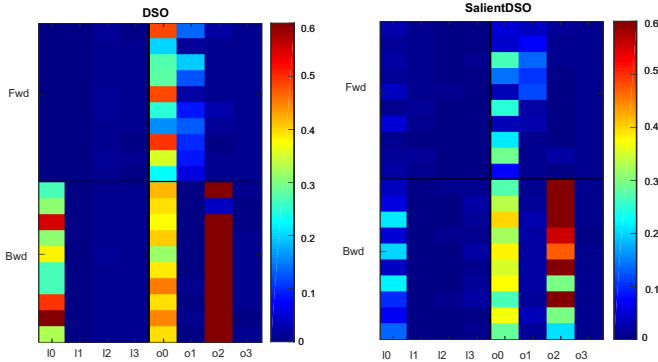


Fig. 5: Comparison of evaluation results for ICL-NIUM dataset. Left: DSO, Right: SalientDSO. Each square corresponds to a color coded error. Note that Salient DSO almost always has lower error than its DSO counterpart.

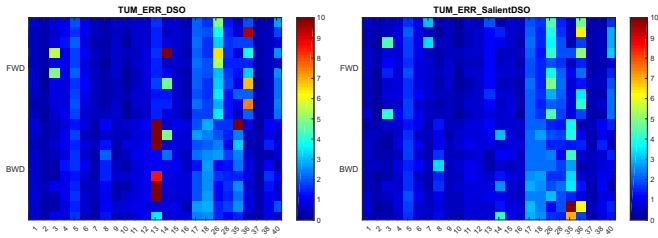


Fig. 6: Comparison of evaluation results for TUM dataset. Left: DSO, Right: SalientDSO. Note that Salient DSO almost always has lower error than its DSO counterpart. Note that, for the TUM dataset scene parsing was turned off as TUM dataset only provides grayscale images and scene parsing outputs are very noisy for grayscale images.

saliency driven features, SalientDSO performs better in accuracy as compared to DSO. We also report alignment error e_{align} on TUM monoVO dataset in Fig. 6. We disable the semantic filtering when we evaluate the proposed method on the TUM monoVO dataset, since this dataset provides only grayscale images and outputs from PSPNet are inaccurate and noisy for grayscale images. In Tables III and IV, we compare our method to DSO and ORB-SLAM on the ICL-NIUM and TUM monoVO datasets. DSO and ORB-SLAM are the current state-of-the-art direct and feature-based monocular VO methods. The results for DSO and ORB-SLAM are taken from [9]. ORB-SLAM is a full-fledged SLAM framework with loop closure and global alignment, while DSO and SalientDSO are merely odometry frameworks. To make the comparison fair, loop-closure detection and re-localization have been turned off for ORB-SLAM. The missing values in the table represent tracking failures. We achieve similar or better performance on most sequences. The improvement is not significant on the TUM monoVO dataset because most of the sequences involve a traversal through a hallway where there are no local salient objects or features for saliency prediction to work well. This makes SalientDSO’s performance close to that of traditional DSO.

TABLE III: RMSE_{ate} on ICL-NIUM dataset in m.

Sequence	Forward			Backward		
	ORB	DSO	SalientDSO	ORB	DSO	SalientDSO
ICL_l0	0.01	0.003	0.022	0.01	-	0.112
ICL_l1	0.02	0.004	0.009	0.04	0.003	0.003
ICL_l2	0.06	0.012	0.004	0.19	0.010	0.005
ICL_l3	0.03	0.006	0.004	0.05	0.008	0.013
ICL_o0	0.21	0.320	0.140	0.41	0.399	0.336
ICL_o1	0.83	0.094	0.055	0.68	0.006	0.020
ICL_o2	0.37	0.012	0.008	0.32	0.582	0.512
ICL_o3	0.65	0.007	0.009	0.06	0.006	0.008
Overall Avg.	0.271	0.057	0.031	0.218	0.144*	0.126

* indicates average taken only on sequences which completed.

TABLE IV: e_{align} on TUM monoVO dataset in m.

Sequence	Forward			Backward		
	ORB	DSO	SalientDSO	ORB	DSO	SalientDSO
seq_01	3.02	0.59	0.60	1.73	0.72	0.60
seq_02	16.12	0.36	0.33	3.23	0.43	0.44
seq_03	3.42	1.75	1.55	1.42	0.59	0.50
seq_04	9.95	0.98	0.82	5.95	1.00	0.76
seq_05	-	1.86	1.77	-	1.55	1.66
seq_06	-	0.97	0.93	1.25	0.73	0.81
seq_07	1.69	0.55	1.14	2.02	0.44	0.48
seq_08	436.00	0.36	0.44	2.63	1.28	1.47
seq_09	2.04	0.65	0.58	0.67	0.52	0.53
seq_10	2.52	0.35	0.34	1.43	0.61	0.61
seq_11	7.20	0.62	0.58	2.99	0.87	0.89
seq_12	2.98	0.75	0.67	3.10	1.01	0.84
seq_13	5.13	1.54	1.27	2.59	8.96	0.81
seq_14	13.27	2.89	0.71	2.10	1.35	1.69
seq_15	2.90	0.71	0.71	1.90	0.88	0.81
seq_16	2.40	0.47	0.45	1.58	0.72	0.67
seq_17	12.29	2.10	2.10	1.50	2.13	2.50
seq_18	14.64	1.77	1.52	-	2.62	2.47
seq_26	28.46	3.98	3.60	4.62	1.66	1.89
seq_28	19.17	1.48	1.88	3.57	1.47	1.65
seq_35	14.09	1.10	0.84	16.81	5.48	9.97
seq_36	1.81	4.01	3.25	1.69	0.70	1.46
seq_37	0.60	0.35	0.40	1.30	0.37	0.46
seq_38	-	0.55	0.50	24.77	1.10	1.03
seq_40	-	2.04	2.16	18.93	0.87	1.04
Overall Avg.	28.55*	1.31	1.17	-	1.52	1.44

* indicates average taken only on sequences which completed.

The claim in the paper is that the usage of visual saliency should result in more robust features than just using image gradient based features as in DSO. The intuition behind this claim is that visual saliency includes high level semantics which inherently make the features more robust. To support this claim, we anticipate that SalientDSO should perform much better than DSO when the number of points is very low (as low as 40 points). To demonstrate this claim, we evaluate on each CVL sequence. We run each sequence in both forward and backward direction 100 times, with an extremely low point density of $N_p = 40$. The results are shown in Table V. We define failure as either an optimization failure or tracking loss. Our proposed method is much more robust and predicts an accurate trajectory, while DSO has a much higher failure rate and its trajectory and projected point cloud shows significant drift in scale and position. An example of trajectory and projected point cloud is shown in Fig. 7. This experiment highlights the robustness of features chosen in SalientDSO for cluttered indoor scenes and how this will be useful for robots with very low computation power due to the less computational and memory requirements when N_p is low.

TABLE V: Comparison of success rate between DSO and SalientDSO on CVL dataset.

Sequence	DSO	SalientDSO
CVL_01_Fwd	53%	65%
CVL_01_Bwd	59%	92%
CVL_02_Fwd	73%	96%
CVL_02_Bwd	71%	91%

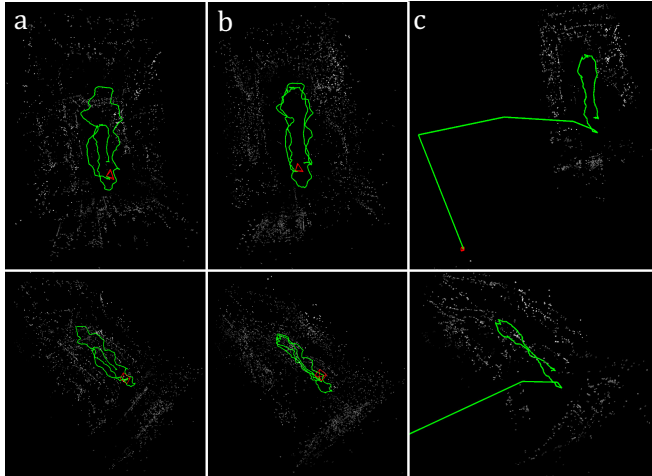


Fig. 7: Comparison of outputs for $N_p = 40$ – very few features. (a) Success case of DSO with a large amount of drift, (b) Success case for SalientDSO, (c) Failure case of DSO where the optimization diverges due to very few features. Notice that SalientDSO can perform very well in these extreme conditions showing the robustness of the features chosen.

B. Qualitative Evaluation

Examples of the reconstructed scenes of sequences CVL_01 and TUM sequence_01 are shown in Figs. 8 and 9 respectively. Although both reconstructed scenes look similar, one could observe that amount of drift in SalientDSO is much less compared to DSO (refer to the zoomed part of Fig. 8). One can clearly observe that the checkerboard of different loops align better in our approach. Instead of sampling random high gradient points, sampling salient and important points improves the robustness of VO. Sampling salient points achieves removing outliers and points with unconstrained depth in optimization which improves the prediction of initial estimates and the output of windowed bundle adjustment in optimization.

V. CONCLUSIONS

We introduce the philosophy of attention and fixation to visual odometry. Based on this philosophy, we develop Salient Direct Sparse Odometry, which brings the concept of attention and fixation based on visual saliency into Visual Odometry to achieve robust feature selection. We provide thorough quantitative and qualitative evaluations on ICL-NUIM and TUM monoVO dataset to demonstrate that using salient features improves the robustness and accuracy. We also collect and publicly release a new CVL dataset with

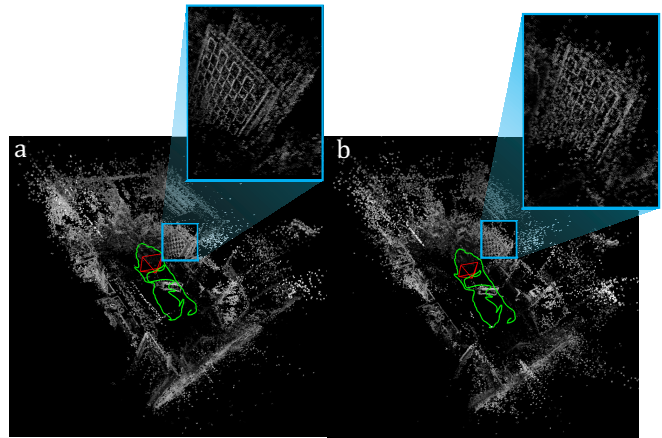


Fig. 8: Comparison of drift. (a) DSO, (b) SalientDSO. Observe that SalientDSO’s output has the checkerboard from different times more closely aligned as compared to DSO. Here $N_p = 1000$.

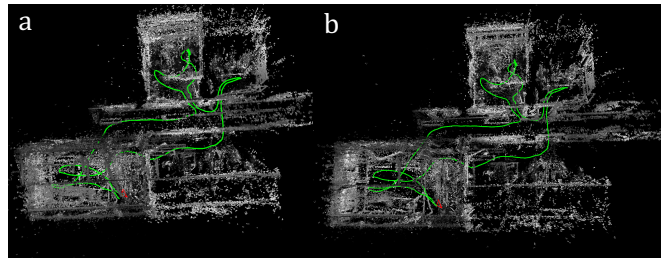


Fig. 9: Sample outputs for TUM sequence_1. (a) DSO, (b) SalientDSO. Here $N_p = 1000$.

cluttered scenes for mapping. We show the robustness of our features by very low drift visual odometry with as low as 40 features per frame. Our method takes about a second per frame for computation of saliency and scene parsing on an NVIDIA Titan-Xp GPU and the remaining computations run real-time at 30fps on an Intel® Core i7 6850K 3.6GHz CPU. In the near future, we plan to extend our method to outdoor environment. We also consider to implement our method on hardware to make the complete pipeline real-time.

ACKNOWLEDGEMENT

This work was partly funded by the Brin Family Foundation, Northrop Grumman Corporation and National Science Foundation under grant SMA 1540917 and grant CNS 1544797.

REFERENCES

- [1] Andrew J Davison, Ian D Reid, Nicholas D Molton, and Olivier Stasse. Monoslam: Real-time single camera slam. *IEEE transactions on pattern analysis and machine intelligence*, 29(6):1052–1067, 2007.
- [2] Georg Klein and David Murray. Parallel tracking and mapping for small ar workspaces. In *Mixed and Augmented Reality, 2007. ISMAR 2007. 6th IEEE and ACM International Symposium on*, pages 225–234. IEEE, 2007.
- [3] Richard A Newcombe, Steven J Lovegrove, and Andrew J Davison. Dtam: Dense tracking and mapping in real-time. In *Computer Vision (ICCV), 2011 IEEE International Conference on*, pages 2320–2327. IEEE, 2011.

- [4] Jakob Engel, Thomas Schöps, and Daniel Cremers. Lsd-slam: Large-scale direct monocular slam. In *European Conference on Computer Vision*, pages 834–849. Springer, 2014.
- [5] R. Mur-Artal, J. M. M. Montiel, and J. D. Tardós. Orb-slam: A versatile and accurate monocular slam system. *IEEE Transactions on Robotics*, 31(5):1147–1163, Oct 2015.
- [6] Jan Stühmer, Stefan Gumhold, and Daniel Cremers. Real-time dense geometry from a handheld camera. In *Joint Pattern Recognition Symposium*, pages 11–20. Springer, 2010.
- [7] Michael Bloesch, Sammy Omari, Marco Hutter, and Roland Siegwart. Robust visual inertial odometry using a direct ekf-based approach. In *Intelligent Robots and Systems (IROS), 2015 IEEE/RSJ International Conference on*, pages 298–304. IEEE, 2015.
- [8] Sebastian A Scherer and Andreas Zell. Efficient onboard rgbd-slam for autonomous mavs. In *Intelligent Robots and Systems (IROS), 2013 IEEE/RSJ International Conference on*, pages 1062–1068. IEEE, 2013.
- [9] J. Engel, V. Koltun, and D. Cremers. Direct sparse odometry. *IEEE Transactions on Pattern Analysis and Machine Intelligence*, Apr 2017.
- [10] Ajay Mishra, Yiannis Aloimonos, and Cheong Loong Fah. Active segmentation with fixation. In *Computer Vision, 2009 IEEE 12th International Conference on*, pages 468–475. IEEE, 2009.
- [11] John Aloimonos et al. Active vision. *International journal of computer vision*, 1(4):333–356, 1988.
- [12] Jeannette Bohg et al. Interactive perception: Leveraging action in perception and perception in action. *IEEE Transactions on Robotics*, 33(6):1273–1291, 2017.
- [13] Ruzena Bajcsy et al. Revisiting active perception. *Autonomous Robots*, pages 1–20, 2017.
- [14] Javier Civera, Dorian Gálvez-López, Luis Riazuelo, Juan D Tardós, and JMM Montiel. Towards semantic slam using a monocular camera. In *Intelligent Robots and Systems (IROS), 2011 IEEE/RSJ International Conference on*, pages 1277–1284. IEEE, 2011.
- [15] Sean L Bowman, Nikolay Atanasov, Kostas Daniilidis, and George J Pappas. Probabilistic data association for semantic slam. In *Robotics and Automation (ICRA), 2017 IEEE International Conference on*, pages 1722–1729. IEEE, 2017.
- [16] Lifeng An, Xinyu Zhang, Hongbo Gao, and Yuchao Liu. Semantic segmentation-aided visual odometry for urban autonomous driving. *International Journal of Advanced Robotic Systems*, 14(5):1729881417735667, 2017.
- [17] Kostas Alexis Tung Dang, Christos Papachristos. Visual saliency-aware receding horizon autonomous exploration with application to aerial robotics. In *Robotics and Automation (ICRA), 2018 IEEE International Conference on*. IEEE, 2018.
- [18] J. Engel, T. Schöps, and D. Cremers. LSD-SLAM: Large-scale direct monocular SLAM. In *European Conference on Computer Vision (ECCV)*, September 2014.
- [19] Stefan Leutenegger, Simon Lynen, Michael Bosse, Roland Siegwart, and Paul Furgale. Keyframe-based visual-inertial odometry using nonlinear optimization. *The International Journal of Robotics Research*, 34(3):314–334, 2015.
- [20] J. Pan, C. Canton Ferrer, K. McGuinness, N. E. O’Connor, J. Torres, E. Sayrol, and X. Giro-i-Nieto. SalGAN: Visual Saliency Prediction with Generative Adversarial Networks. *ArXiv e-prints*, January 2017.
- [21] Ian Goodfellow, Jean Pouget-Abadie, Mehdi Mirza, Bing Xu, David Warde-Farley, Sherjil Ozair, Aaron Courville, and Yoshua Bengio. Generative adversarial nets. In Z. Ghahramani, M. Welling, C. Cortes, N. D. Lawrence, and K. Q. Weinberger, editors, *Advances in Neural Information Processing Systems 27*, pages 2672–2680. Curran Associates, Inc., 2014.
- [22] K. Simonyan and A. Zisserman. Very Deep Convolutional Networks for Large-Scale Image Recognition. *ArXiv e-prints*, September 2014.
- [23] J. Deng, W. Dong, R. Socher, L.-J. Li, K. Li, and L. Fei-Fei. ImageNet: A Large-Scale Hierarchical Image Database. In *CVPR09*, 2009.
- [24] Ming Jiang, Shengsheng Huang, Juanyong Duan, and Qi Zhao. Salicon: Saliency in context. In *The IEEE Conference on Computer Vision and Pattern Recognition (CVPR)*, June 2015.
- [25] H. Zhao, J. Shi, X. Qi, X. Wang, and J. Jia. Pyramid scene parsing network. In *2017 IEEE Conference on Computer Vision and Pattern Recognition (CVPR)*, volume 00, pages 6230–6239, July 2017.
- [26] A. Handa, T. Whelan, J.B. McDonald, and A.J. Davison. A benchmark for RGB-D visual odometry, 3D reconstruction and SLAM. In *IEEE Intl. Conf. on Robotics and Automation, ICRA*, Hong Kong, China, May 2014.
- [27] J. Engel, V. Usenko, and D. Cremers. A Photometrically Calibrated Benchmark For Monocular Visual Odometry. *ArXiv e-prints*, July 2016.
- [28] Parrot SLAMDunk. <http://developer.parrot.com/docs/slamdunk/>, 2018.